Journal of Alloys and Compounds 509 (2011) 10086–10091

Contents lists available at ScienceDirect

Journal of Alloys and Compounds

journal homepage: www.elsevier.com/locate/jallcom

Enhanced photocatalytic degradation of methylene blue by ZnO-reduced graphene oxide composite synthesized via microwave-assisted reaction

Tian Lv, Likun Pan*, Xinjuan Liu, Ting Lu, Guang Zhu, Zhuo Sun

Engineering Research Center for Nanophotonics and Advanced Instrument, Ministry of Education, Department of Physics, East China Normal University, Shanghai, 200062 China

ARTICLE INFO

Article history:
Received 9 April 2011
Received in revised form 5 August 2011
Accepted 9 August 2011
Available online 16 August 2011

Keywords:
ZnO
Reduced graphene oxide
Microwave-assisted reaction
Photocatalysis

ABSTRACT

A quick and facile microwave-assisted reaction is used to synthesize ZnO-reduced graphene oxide (RGO) hybrid composites by reducing graphite oxide dispersion with zinc nitrate using a microwave synthesis system. Their photocatalytic performance in degradation of methylene blue is investigated and the results show that the RGO plays an important role in the enhancement of photocatalytic performance and the ZnO–RGO composite with 1.1 wt. % RGO achieves a maximum degradation efficiency of 88% in a neutral solution under UV light irradiation for 260 min as compared with pure ZnO (68%) due to the increased light absorption, the reduced charge recombination with the introduction of RGO.

© 2011 Elsevier B.V. All rights reserved.

1. Introduction

Photocatalytic degradation of organic pollutants for water treatment has attracted wide attention due to its effectiveness, easy operation and ideally producing nontoxic end products [1–6]. Photocatalysis is normally based on the light absorption of semiconductor oxide photocatalyst, typically ZnO [6] or TiO_2 [5], to excite the electrons from valence band to conduction band and create electron-hole pairs [7]. These electrons and holes can migrate and initiate redox reactions with water and oxygen, and then degrade organic molecules absorbed on the surface of the photocatalyst. Currently a major limitation to achieve high photocatalytic efficiency is the quick recombination of photo-generated charge carries [8]. Recombination has faster kinetics than surface redox reactions and greatly reduces the quantum efficiency of photocatalysis. Therefore, to enhance the photocatalytic efficiency, it is essential to retard the recombination of the charge carriers. Currently a particularly attractive option is to design and develop hybrid materials based on semiconductor oxide to solve the above problem [9–13]. Zhu et al. [14] coated ZnO nanoparicles on carbon nanotubes (CNTs) via a sol process using zinc acetate precursor and the ZnO–CNTs composite exhibited a high photocatalytic activity in degradation of methyl orange. Jiang and Gao [15] deposited ZnO nanoparticles on CNTs through noncovalent modification of CNTs with sodium dodecyl sulfate for photocatalytic degradation of methylene blue (MB) and a degradation efficiency of ~85% was achieved. Mu et al. [16] obtained ZnO-carbon nanofibers (CNFs) heteroarchitectures by a combination of electrospinning technique and hydrothermal process and the ZnO-CNFs heteroarchitectures showed a high efficiency in the photocatalytic degradation of rhodamine B. In photocatalysis process, CNTs or CNFs can act as an excellent electron-acceptor/transport material to effectively facilitate the migration of photo-induced electrons and hinder the charge recombination in electron-transfer processes due to the electronic interaction between semiconductor oxide and CNTs, which enhances the photocatalytic performance.

Recently, graphene, a rising star in carbon family, has generated increasing interest both in fundamental science and for wide potential applications due to its excellent electronic properties, superior chemical stability and high specific surface area [17,18]. Similar to CNTs, graphene can also act as an excellent electron-acceptor/transport material [19–21] and attempts to combine semiconductor oxide photocatalyst and graphene have been reported in efforts to obtain hybrid materials with superior photocatalytic performance [22–30]. Li and Cao [31] reported the incorporation of graphene in ZnO to form ZnO–graphene composite by chemically reducing the mixture of graphite oxide (GO) dispersion and $Zn(AcO)_2$ in aqueous solution using $NaBH_4$ and studied its significant influence on photocatalytic degradation of rhodamine B under UV and visible light irradiation. Xu et al. [19] synthesized ZnO–graphene composite by reducing GO coated on the surface of ZnO nanoparticles using hydrazine and found that the ZnO–graphene composite showed an improved photocatalytic efficiency (~90%) in the degradation of MB as compared with pure ZnO. Akhavan et al. [32] reported the incorporation of graphene in TiO_2 to form TiO_2-graphene composite by UV-light

* Corresponding author. Tel.: +86 21 62234132; fax: +86 21 62234321.
E-mail address: lkpan@phy.ecnu.edu.cn (L. Pan).

0925-8388/$ – see front matter © 2011 Elsevier B.V. All rights reserved.
doi:10.1016/j.jallcom.2011.08.045

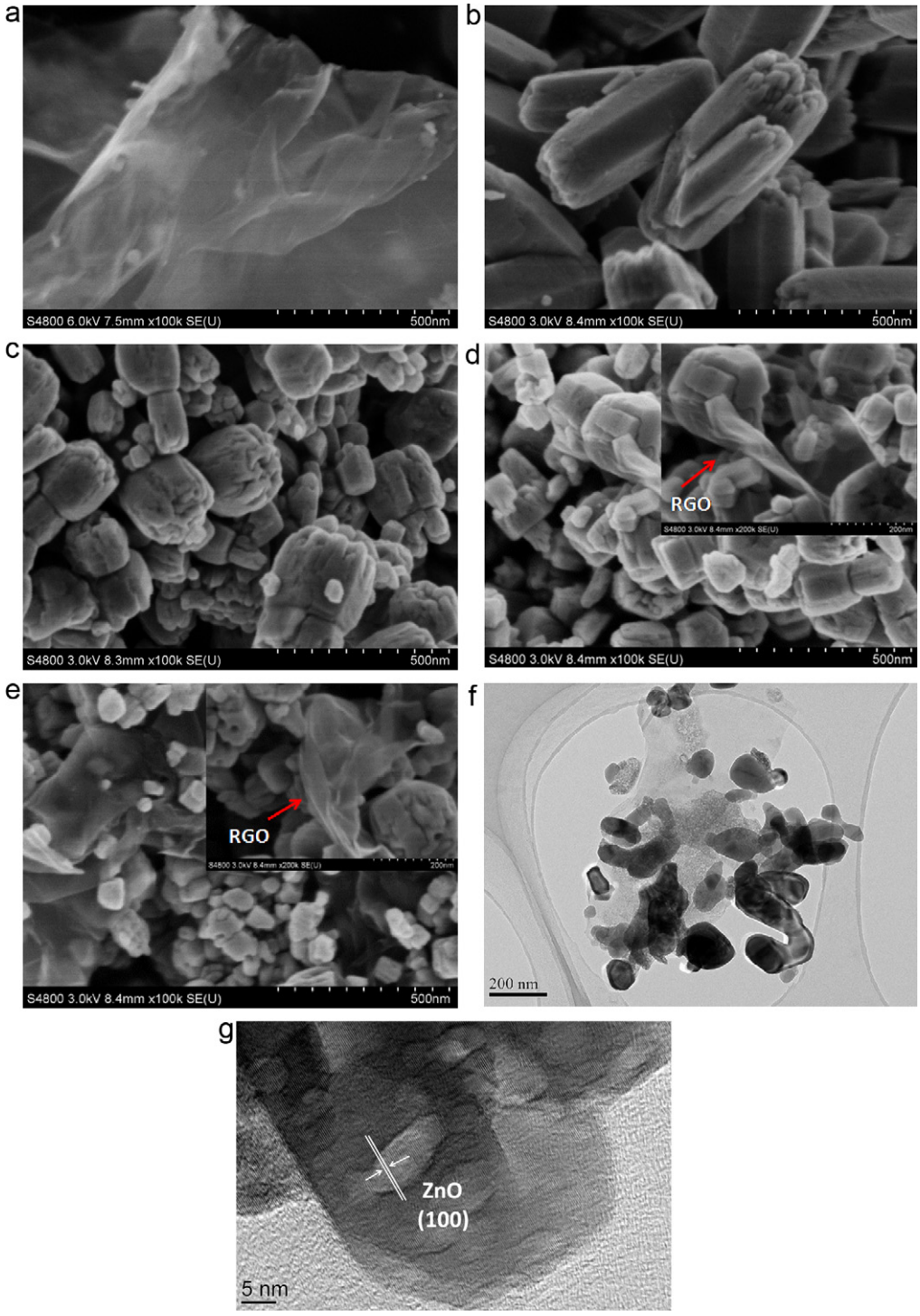

Fig. 1. FESEM images of (a) RGO, (b) ZnO, (c) ZG-2, (d) ZG-3 and (e) ZG-4; (e) low-magnification and (f) high-magnification HRTEM images of ZG-2.

photocatalytic reduction of GO. Zhou et al. [33] prepared TiO_2–graphene composites through a one-pot solvothermal reaction by using GO and tetrabutyl titanate as starting materials with excellent photocatalysis to MB degradation under irradiation of simulated sunlight. Zhang et al. [34] obtained TiO_2–graphene composite from reduction of the mixture of GO and TiO_2 by heat treatment and the visible light photocatalytic activity of the composite was enhanced greatly on decomposition of MB. However, as promising hybrid materials for photocatalysis, the exploration on semiconductor oxide photocatalyst–graphene composite is not nearly enough so far. Especially as an inexpensive, quick, versatile technique, microwave-assisted reaction is seldom employed to synthesize semiconductor oxide-reduced graphene oxide (RGO) hybrid composite materials for photocatalysis although such a method has been used successfully to fabricate RGO [35–37], ZnO [38–40] and TiO_2 [41].

In this work, one-step synthesis of ZnO–RGO composite was carried out through microwave-assisted reduction of GO dispersion with zinc nitrate using a microwave system. Microwave irradiation can heat the reactant to a high temperature in a short time by transferring energy selectively to microwave absorbing polar solvents. Thus it can facilitate mass production in a short time with little

energy cost [42–45] and form an intimate contact between ZnO and RGO [46,47]. Here ZnO–RGO is selected to study because ZnO has higher photocatalytic efficiencies, faster degradation rates and lower cost than TiO_2 in removal of most of dyes [48–50]. ZnO–RGO composite exhibited an enhanced photocatalytic performance in degradation of MB under UV light irradiation as compared with pure ZnO.

2. Experimental

2.1. Synthesis of ZnO–RGO composite

Commercial graphite powder was used as the starting reagent for the synthesis of GO via modified Hummers method, which has been described in our previous works [51–54]. A certain amount of 1.8 mg/ml GO suspension was added into 20 ml 0.3 M $Zn(NO_3)_2$ solution and then the solution was sonicated for 30 min to produce uniform dispersion. A dilute NaOH solution was dropped in the solution to form a brownish-black suspension with a pH value of 10–11. The solution was then put into an automated focused microwave system (Explorer-48, CEM Co.) and treated for 30 min at 100 °C. It was obviously found that the color of suspension had changed into grayish-black, indicating the chemical reduction of the GO sheets [55]. The as-synthesized ZnO–RGO samples with 0.3, 0.7, 1.1, 1.5 and 1.8 wt. % RGO, named as ZG-1, ZG-2, ZG-3, ZG-4 and ZG-5, were isolated by filtration, washed for several times with distilled water, and finally dried in a vacuum oven at 60 °C for 24 h. Pure RGO and ZnO were also synthesized by direct microwave assisted reaction for comparison.

Microwave-assisted synthesis of ZnO–RGO composite is a one-step process. Under acidic condition of pH < 6.0, Zn element exists as Zn^{2+} and $ZnOH^+$ soluble ions in the aqueous solution [47,56]. Zn^{2+} and $ZnOH^+$ ions could be tightly adsorbed onto the both sides of GO due to the functional groups such as carboxyl, hydroxyl and epoxy groups on the surface of GO. With the increase of pH value, a conversion from Zn^{2+} and $ZnOH^+$ ions to $Zn(OH)_2$ precipitation happens and finally GO is reduced to RGO and the $Zn(OH)_2$ is transformed to ZnO particles on the both sides of RGO under microwave heating.

2.2. Characterization

The surface morphology, structure and composition of the samples were characterized by field-emission scanning electron microscopy (FESEM, Hitachi S-4800), high-resolution transmission electron microscopy (HRTEM, JEOL-2010), atomic force microscopy (AFM, Veeco Dimension 3100), Fourier transform infrared spectroscopy (FTIR, Zetasizer Nano ZS) analysis and X-ray diffraction spectroscopy (XRD, Holland Panalytical PRO PW3040/60) with Cu Kα radiation (V = 30 kV, I = 25 mA), respectively. The UV–vis absorption spectra were recorded using a Hitachi U-3900 UV–vis spectrophotometer. The pH value of the suspension was adjusted between 5 and 11 by adding HCl or NaOH and the isoelectric point (IEP) was measured using a Zeta Meter (JS94J, Powereach).

2.3. Photocatalytic experiments

The photocatalytic performance of the as-prepared samples was evaluated by photocatalytic degradation of MB under UV light irradiation. The samples (1.5 g/l) were dispersed in the 100 ml MB aqueous solution (5 mg/l). The mixed suspensions were magnetically stirred for 0.5 h in the dark to reach an adsorption–desorption equilibrium. Under ambient conditions and stirring, the mixed suspensions were exposed to UV irradiation produced by a 500 W high pressure Hg lamp with the main wave crest at 365 nm. At certain time intervals, 2 ml of the mixed suspensions were extracted and centrifugated to remove the photocatalyst. The degradation process was monitored by measuring the absorption of MB in filtrate at 663 nm using UV–vis absorption spectrometer. It is known that one of the major drawbacks of ZnO photocatalyst is its photo-instability in aqueous solution due to its photocorrosion under UV irradiation, which significantly decreases the photocatalytic activity of ZnO. Therefore, the photo-stability of as-prepared sample was examined for degradation of MB during a three-cycle experiment.

3. Results and discussion

The FESEM images of RGO, pure ZnO, ZG-2, ZG-3 and ZG-4 are shown in Fig. 1(a)–(e). The RGO nanosheets are curled and corrugated. The ZnO displays a hexagonal nanorod structure and its length and diameter decrease with the increase of RGO content in the composite, which implies that the presence of RGO inhibits the growth of ZnO nanorods [57]. It is observed that the RGO sheets with wrinkles and folds are decorated densely by the ZnO nanorods. The low-magnification and high-resolution HRTEM images of ZG-2 are shown in Fig. 1(f) and (g). The large crystallites are identified to be ZnO nanorods. The lattice spacing measured for the crystalline plane is 0.28 nm, corresponding to the (1 0 0) plane of ZnO (JPCDS 79-0206) [58].

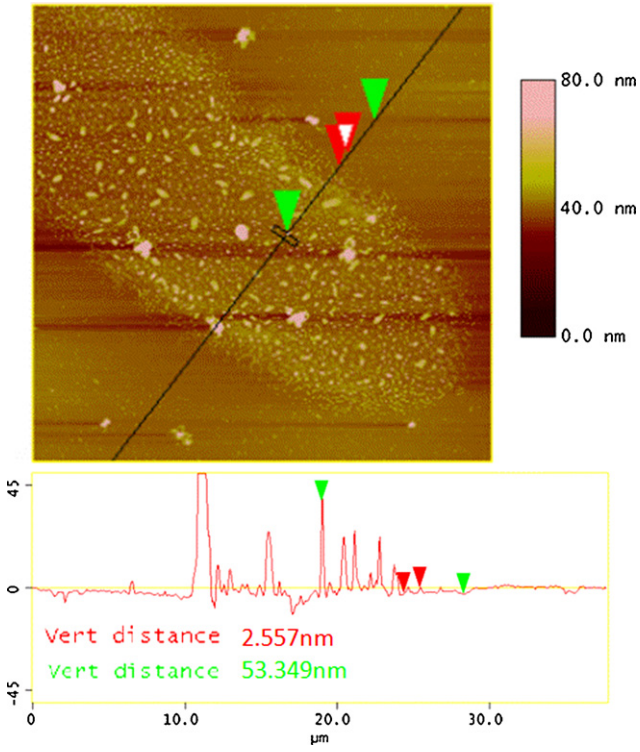

Fig. 2. AFM image of ZG-3: topography image and height profiles obtained from positions indicated by different triangle symbols (red: RGO; green: ZnO–RGO). (For interpretation of the references to color in this figure legend, the reader is referred to the web version of the article.)

To indicate the acquirement of RGO, an aqueous solution of ZnO–RGO was dropped onto the hydrophilic-treated silicon for AFM measurements. Fig. 2 shows the AFM image of as-prepared ZG-3. It is observed that ZnO is attached onto the surface of RGO sheet, which is demonstrated in the height profile diagram containing the sharp peaks with the height of ~50 nm. The profile also shows that the thickness of the RGO is 2.557 nm, corresponding to the RGO of four or five layers based on theoretical values of 0.78 nm for single layer RGO and the thickness contribution from oxygen-containing groups on the surfaces [47,51].

Fig. 3 shows the FTIR spectra of GO, RGO, ZnO, and ZG-3. There is a great decrease in the intensities of C=O (1627 cm^{-1}),

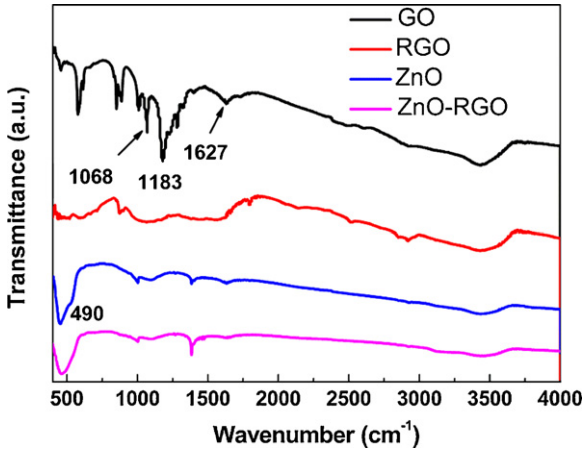

Fig. 3. FTIR spectra of GO, RGO, ZnO and ZG-3.

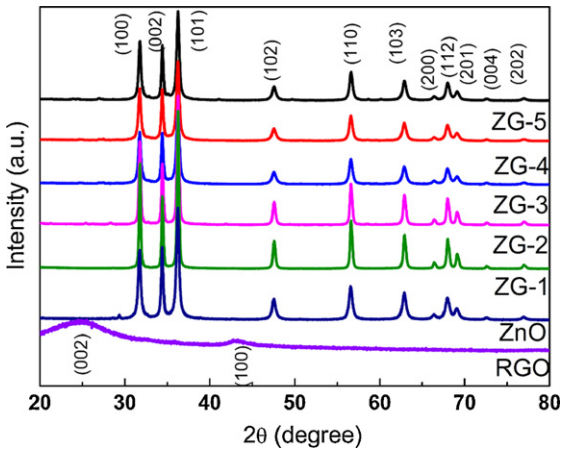

Fig. 4. XRD patterns of RGO, ZnO, ZG-1, ZG-2, ZG-3, ZG-4 and ZG-5.

C–OH (1183 cm^{-1}) and C-O (1068 cm^{-1}) stretching vibration peaks in RGO compared to those in GO, which suggests that microwave-assisted reduction is an effective method to remove oxygen-containing groups of GO. The absorption band at 490 cm^{-1} of ZG-3 is similar to that of pure ZnO, which is owing to stretching models of Zn–O [59].

The XRD patterns of RGO, ZnO, ZG-1, ZG-2, ZG-3, ZG-4 and ZG-5 are shown in Fig. 4. The RGO nanosheets exhibit a (0 0 2) diffraction peak at 26° and a (1 0 0) peak at 44.5° [60]. The main diffraction peaks of ZnO–RGO composites are similar to that of pure ZnO and correspond to the hexagonal phase of ZnO (JPCDS 36-1451), which indicates that the presence of RGO does not result in the development of new crystal orientations or change in preferential orientations of ZnO. No typical diffraction peaks of carbon species are observed, which may be due to the low amount and relatively low diffraction intensity of RGO in the composite [61].

The UV–vis absorption spectra of RGO, ZnO, ZG-1, ZG-2, ZG-3, ZG-4 and ZG-5 are shown in Fig. 5. It is observed that the RGO exhibits a strong absorption peak at 265 nm which is regarded as the excitation of π-plasmon of graphitic structure [58]. The sharp characteristic absorption peak at 365 nm indicates the existence of good crystalline and impurity suppressed ZnO nanorods [62]. It is observed that the absorbance of the ZnO–RGO composite increases even in visible light region with the increase of RGO content in the composite, which is similar to those reported in hybridization of TiO_2 with graphite-like carbon layers or RGO [23,33,63]. The presence of RGO induces the increased light absorption intensity, which may be due to the increase of surface electric charge of the oxides in the ZnO–RGO composite and the modification of the fundamental

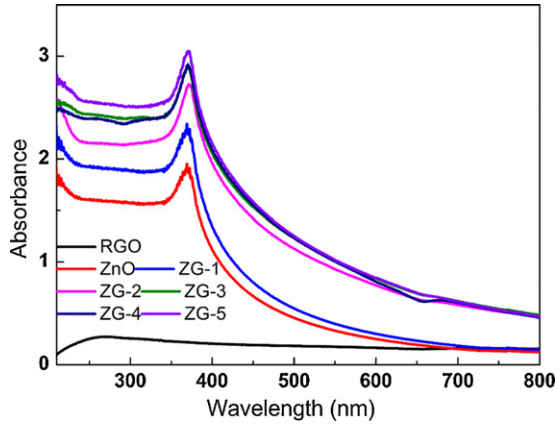

Fig. 5. UV–vis absorption spectra of RGO, ZnO, ZG-1, ZG-2, ZG-3, ZG-4 and ZG-5.

Table 1
Effect of photocatalyst dosage on photocatalytic degradation of MB using pure ZnO.

C_{ZnO} (g/l)	0.5	1.0	1.5	2
Degradation efficiency (%)	53	60	68	47

process of electron–hole pair formation during irradiation [64]. In addition, the small red shift of absorption edge as compared to pure ZnO should be ascribed to the chemical bonding between ZnO and RGO, which is similar to the result in the case of TiO_2–RGO composite materials [24,25,33].

The effect of photocatalyst dosage on the photocatalytic degradation of MB using pure ZnO was tested and the results are shown in Table 1. It can be seen that the degradation efficiency increases from 53% to 68% with the increasing dosage of ZnO photocatalyst from 0.5 to 1.5 g/l due to the increase of the photogenerated electron–hole pairs which lead to the destruction of more MB molecules. However, when the ZnO amount is further increased, the photocatalytic performance deteriorates. It is because that when the photocatalyst dosage is increased above a certain value, the solution transparence is crippled and scattering effect happens. Correspondingly the light utilization rate is reduced which lowers the photocatalytic activity of ZnO. Thus, photocatalyst dosage is selected to be 1.5 g/l in this work.

The photocatalytic degradation of MB under UV irradiation was used to evaluate the photocatalytic performance of ZnO, ZG-1, ZG-2, ZG-3, ZG-4 and ZG-5, as shown in Fig. 6. It is observed that the concentration of MB is hardly reduced under UV light irradiation in the absence of the photocatalyst. As shown in the inset of Fig. 6, when ZnO photocatalyst is used, the UV–vis absorption peak of MB at 663 nm, related to the concentration of MB in the solution, becomes weak with the increase of the time under UV light irradiation. After 260 min, the degradation efficiency is calculated to be 68%. When RGO is introduced into ZnO, the degradation efficiency is increased to 72% and 77% for ZG-1 and ZG-2 and reaches a maximum value of 88% for ZG-3. It is known that during photocatalysis, the light absorption and the charge transportation and separation are crucial factors [24]. The enhancement of the photocatalytic performance should be mainly ascribed to the increase of the light absorption with the presence of RGO in ZnO and the stepwise structure of energy levels constructed in the ZnO–RGO composite [20,30,65,66]. The relevant band positions of ZnO (conduction band: −4.05 eV vs. vacuum [20]) and RGO (work function: −4.42 eV [67,68]) favor the transfer and separation of photo-induced electrons from ZnO conduction band to RGO and hinder the charge recombination in

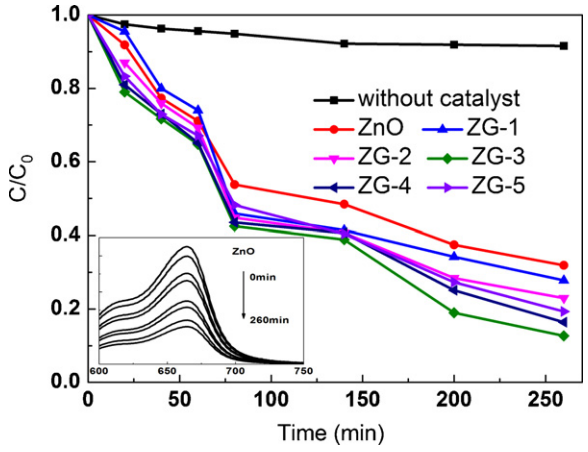

Fig. 6. Photocatalytic degradation of MB by ZnO, ZG-1, ZG-2, ZG-3, ZG-4 and ZG-5 under UV light irradiation. The inset shows the UV-vis absorbance of MB with the time during photocatalytic degradation under UV light irradiation using pure ZnO. The concentrations of MB and photocatalyst are 5 mg/l and 1.5 g/l, respectively.

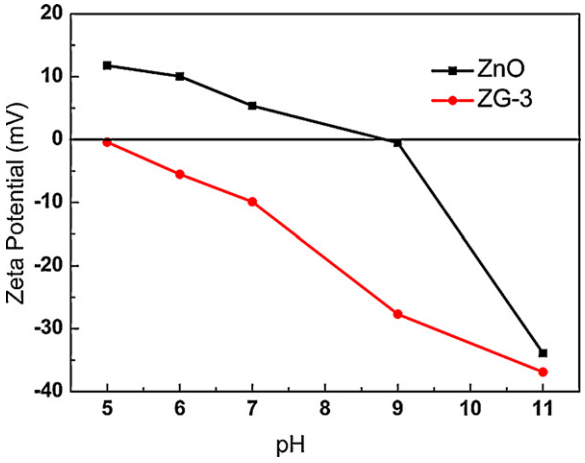

Fig. 7. Zeta potential of ZnO and ZG-3 as a function of pH value.

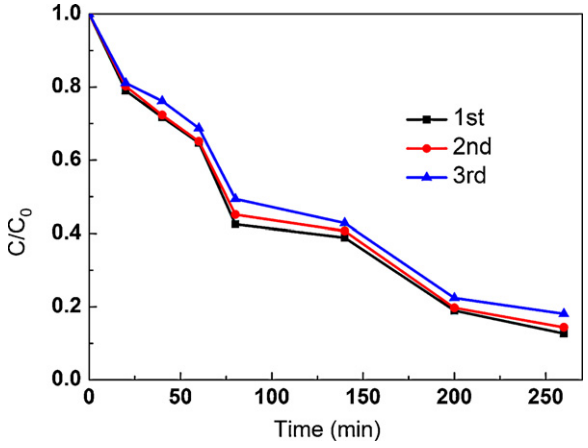

Fig. 9. Photo-stability of ZG-3 by investigating its photocatalytic activity under UV light irradiation with three times of cycling uses.

electron-transfer processes. Furthermore, the incorporation of RGO can facilitate a better platform for adsorption of MB [30], which can be confirmed by the IEP measurement in Fig. 7. The IEP of ZnO is found at pH of around 9, which is similar to that reported by others [69]. However, the IEP of ZG-3 shifts to lower pH value, indicating that acidic functional groups are present in ZnO–RGO composites and can favor the electrostatic adsorption of the cationic MB and increase the photocatalytic performance [70]. When the RGO content is further increased above its optimum value, the photocatalytic performance deteriorates. This is due to the following reasons: (i) RGO can absorb some UV light and thus there exists a light harvesting competition between ZnO and RGO with increase of RGO amount [19,71]; (ii) the excessive RGO can act as a kind of recombination center instead of providing an electron pathway [23,54,68].

Fig. 8 shows the effect of pH value on the photocatalytic activity of ZG-3 photocatalyst. It can be observed that the pH value can significantly affect the photocatalytic activity of ZnO-RGO photocatalyst. The degradation efficiency is significantly increased from 68.5% to 88% with the increase of pH value from 5 to 7 and reaches maximally 91.7% at pH of 9 because more cationic MB is absorbed onto the photocatalyst surface with negative charge when the pH value is above its IEP. Such an efficiency in degradation of MB is comparable to the ones for ZnO–CNTs [15] and ZnO–RGO composite synthesized using hydrazine [19]. However, the degradation efficiency decreases when pH value is further increased to 11, which should be ascribed to the instability of ZnO in strong alkali condition.

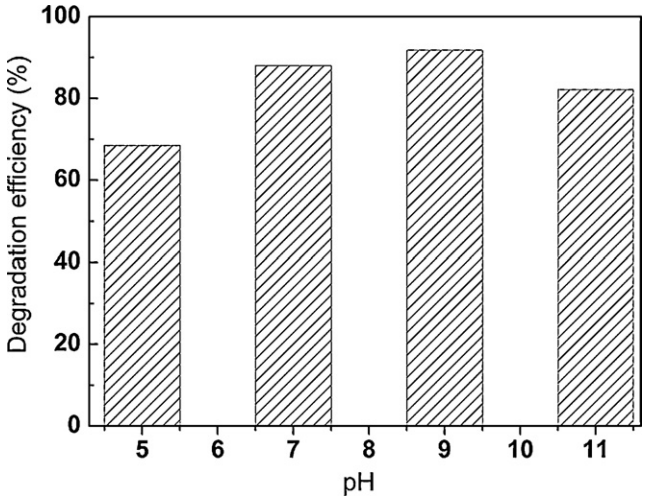

Fig. 8. Effect of solution pH value on the degradation efficiency of MB in the presence of ZG-3.

The photo-stability of ZG-3 by investigating its photocatalytic activity under UV light irradiation at pH of 7 with three times of cycling uses was studied, as shown in Fig. 9. It can be seen that the recycled use of ZG-3 for three times does not conspicuously affect its photocatalytic activity. Apparently, the composite is stable under the studied conditions and the photocorrosion effect of ZnO was effectively inhibited by RGO after hybridized [72].

4. Conclusions

ZnO–RGO composites are successfully synthesized via microwave-assisted reduction of GO dispersion with zinc nitrate. The results of photocatalytic experiments indicate that the incorporation of RGO can enhance the photocatalytic performance and photo-stability of ZnO in degradation of MB and the ZnO–RGO composite with 1.1 wt. % RGO achieves a degradation efficiency of 88% at pH of 7 and 91.7% at pH of 9. The increased light absorption and the reduced charge recombination with the introduction of RGO are responsible for the enhanced photocatalytic activity of the ZnO–RGO composite.

It should be noticed that the photocatalytic performance of ZnO–RGO composites synthesized via microwave-assisted reaction is believed to be further improved by optimizing the microwave reaction conditions such as the reaction time and temperature, the microwave power and the precursor solution. The present synthetic strategy should be a promising fabrication technique for a simple, rapid and effective mass production of the composite photocatalysts for the efficient removal of pollutants.

Acknowledgements

This work was supported by Special Project for Nanotechnology of Shanghai (no. 1052nm02700).

References

[1] P. Ma, Y. Wu, Z. Fu, W. Wang, J. Alloys Compd. 509 (2011) 3576.
[2] W.M. Hou, Y. Ku, J. Alloys Compd. 509 (2011) 5913.
[3] D. Zhang, X. Liu, X. Wang, J. Alloys Compd. 509 (2011) 4972.
[4] M.Y. Guo, M.K. Fung, F. Fang, X.Y. Chen, A.M.C. Ng, A.B. Djurisic, W.K. Chan, J. Alloys Compd. 509 (2011) 1328.
[5] Y. Liao, W. Que, Z. Tang, W. Wang, W. Zhao, J. Alloys Compd. 509 (2011) 1054.
[6] O. Akhavan, M. Mehrabian, K. Mirabbaszadeh, R. Azimirad, J. Phys. D: Appl. Phys. 42 (2009) 225305.
[7] M. Guo, Y. Dai, Chem. Mater. 225 (2010) 528.

[8] R.M. Asmussen, M.T.A. Chen, Environ. Sci. Technol. 43 (2009) 5100.
[9] Y. Xu, H. Xu, H. Li, J. Xia, C. Liu, L. Liu, J. Alloys Compd. 509 (2011) 3286.
[10] Y. Liu, J. Hu, J. Li, J. Alloys Compd. 509 (2011) 5152.
[11] N.M. Mahmoodi, M. Arami, J. Zhang, J. Alloys Compd. 509 (2011) 4754.
[12] Q. Li, C. Zhang, J. Li, J. Alloys Compd. 509 (2011) 1953.
[13] C. Tian, Q. Zhang, B. Jiang, G. Tian, H. Fu, J. Alloys Compd. 509 (2011) 6935.
[14] L.P. Zhu, G.H. Liao, W.Y. Huang, L.L. Ma, Y. Yang, Y. Yu, S.Y. Fu, Mater. Sci. Eng. B 163 (2009) 194–198.
[15] L. Jiang, L. Gao, Mater. Chem. Phys. 91 (2005) 313.
[16] J. Mu, C. Shao, Z. Guo, Z. Zhang, M. Zhang, P. Zhang, B. Chen, Y. Liu, ACS Appl. Mater. Interfaces 3 (2011) 590.
[17] K.S. Novoselov, A.K. Geim, S.V. Morozov, D. Jiang, Y. Zhang, S.V. Dubonos, I.V. Grigorieva, A.A. Firsov, Science 306 (2004) 666.
[18] B. Wang, Y. Wang, J. Park, H. Ahn, G. Wang, J. Alloys Compd. 509 (2011) 7778.
[19] T.G. Xu, L.W. Zhang, H.Y. Cheng, Y.F. Zhu, Appl. Catal. B: Environ. 101 (2011) 382.
[20] B.J. Li, H.Q. Cao, J. Mater. Chem. 21 (2011) 3346.
[21] O. Akhavan, E. Ghaderi, J. Phys. Chem. C 113 (2009) 20214.
[22] O. Akhavan, ACS Nano 4 (2010) 4174.
[23] J. Liu, H. Bai, Y. Wang, Z. Liu, X. Zhang, D.D. Sun, Adv. Funct. Mater. 20 (2010) 4175.
[24] Y. Zhang, Z.R. Tang, X. Fu, Y.J. Xu, ACS Nano 4 (2010) 7303.
[25] O. Akhavan, Carbon 49 (2011) 11.
[26] J. Du, X. Lai, N. Yang, J. Zhai, D. Kisailus, F. Su, D. Wang, L. Jiang, ACS Nano 5 (2011) 590.
[27] D.H. Yoo, T.V. Cuong, V.H. Pham, J.S. Chung, N.T. Khoa, E.J. Kim, S.H. Hahn, Curr. Appl. Phys. 11 (2011) 805.
[28] Y. Yang, L. Ren, C. Zhang, S. Huang, T. Liu, ACS Appl. Mater. Interfaces 3 (2011) 2779.
[29] N. Li, G. Liu, C. Zhen, F. Li, L. Zhang, H.M. Cheng, Adv. Funct. Mater. 21 (2011) 1717.
[30] H. Zhang, X. Lv, Y. Li, Y. Wang, J. Li, ACS Nano 4 (2010) 380.
[31] J. Li, H.Q. Cao, J. Mater. Chem. 21 (2011) 3346.
[32] O. Akhavan, M. Abdolahad, A. Esfandiar, M. Mohatashamifar, J. Phys. Chem. C 114 (2010) 12955.
[33] K. Zhou, Y. Zhu, X. Yang, X. Jiang, C. Li, New J. Chem. 35 (2011) 353.
[34] Y. Zhang, C. Pan, J. Mater. Sci. 46 (2011) 2622.
[35] J. Long, M. Fang, G. Chen, J. Mater. Chem. 21 (2011) 10421.
[36] Z. Xu, H. Li, W. Li, G. Cao, Q. Zhang, K. Li, Q. Fu, J. Wang, Chem. Commun. 47 (2011) 1166.
[37] S.H. Park, S.M. Bak, K.H. Kim, J.P. Jegal, S.I. Lee, J. Lee, K.B. Kim, J. Mater. Chem. 21 (2011) 680.
[38] J.J. Hassan, Z. Hassan, H. Abu-Hassan, J. Alloys Compd. 509 (2011) 6711.
[39] Y.C. Chen, S.L. Lo, Chem. Eng. J. 170 (2011) 411.
[40] A. Kothari, T.K. Chaudhuri, Mater. Lett. 65 (2011) 847.
[41] P. Pradeepan, N. Leyland, D.E. McCormack, J. Colreavy, D. Corr, S.C. Pillai, J. Mater. Chem. 20 (2010) 3650.
[42] H. Wu, P. Cao, W. Li, N. Ni, L. Zhu, X. Zhang, J. Alloys Compd. 509 (2011) 1261.
[43] R. Dwivedi, A. Maurya, A. Verma, R. Prasad, K.S. Bartwal, J. Alloys Compd. 509 (2011) 6848.
[44] G.V. Bazuev, A.P. Tyutyunnik, I.F. Berger, I.V. Nikolaenko, B.G. Golovkin, J. Alloys Compd. 509 (2011) 6158.
[45] G. Zhu, L.K. Pan, T. Xu, Z. Sun, ACS Appl. Mater. Interfaces 3 (2011) 1472.
[46] G. Zhu,, L.K. Pan,, T. Xu, Q.F. Zhao, B. Lu, Z. Sun, Nanoscale 3 (2011) 2188.
[47] T. Lu, L.K. Pan, H.B. Li, G. Zhu, T. Lv, X.J. Liu, Z. Sun, T. Chen, D.H.C. Chua, J. Alloys Compd. 509 (2011) 5488.
[48] F. Lu, W.P. Cai, Y.G. Zhang, Adv. Funct. Mater. 18 (2008) 1047.
[49] S. Sakthivel, B. Neppolian, M.V. Shankar, B. Arabindoo, M. Palanichamy, V. Murugesan, Sol. Energy Mater. Sol. Cells 77 (2003) 65.
[50] N. Daneshvar, D. Salari, A.R. Khataee, J. Photochem. Photobiol. A 162 (2004) 317.
[51] H.B. Li, T. Lu, L.K. Pan, Y.P. Zhang, Z. Sun, J. Mater. Chem. 19 (2009) 6773.
[52] T. Lu,, Y.P. Zhang,, H.B. Li,, L.K. Pan,, Y.L. Li,, Z. Sun,, Electrochim. Acta 55 (2010) 4170.
[53] H.B. Li, L.K. Pan, T. Lu, Y.K. Zhan, C.Y. Nie, Z. Sun, J. Electroanal. Chem. 653 (2011) 40.
[54] G. Zhu,, T. Xu,, T. Lv,, L.K. Pan,, Q.F. Zhao,, Z. Sun,, J. Electroanal. Chem 650 (2011) 248.
[55] H.A. Becerril, J. Mao, Z. Liu, R.M. Stoltenberg, Z. Bao, Y. Chen, ACS Nano 2 (2008) 463.
[56] X. Chen, Y. He, Q. Zhang, L. Li, D. Hu, T. Yin, J. Mater. Sci. 45 (2010) 953.
[57] S.K. Park, J.H. Park, K.Y. Ko, S. Yoon, K.S. Chu, W. Kim, Y.R. Do, Cryst. Growth Des. 9 (2009) 3615.
[58] J.L. Wu, X.P. Shen, L. Jiang, K. Wang, K.M. Chen, Appl. Surf. Sci. 256 (2010) 2826.
[59] N. Lepot, M.K. Van Bael, H. Van den Rul, J. D'Haen, R. Peeters, D. Franco, J. Mullens, Mater. Lett. 61 (2007) 2624.
[60] L. Tang, Y. Wang, Y. Li, H. Feng, J. Lu, J. Li, Adv. Funct. Mater. 19 (2009) 2782.
[61] Y.L. Chen, Z.A. Hu, Y.Q. Chang, H.W. Wang, Z.Y. Zhang, Y.Y. Yang, H.Y. Wu, J. Phys. Chem. C 115 (2011) 2563.
[62] Y. Guo, H.S. Wang, C.L. He, L.J. Qiu, X.B. Cao, Langmuir 25 (2009) 4678.
[63] Y.J. Wang, R. Shi, J. Lin, Y.F. Zhu, Appl. Catal. B: Environ. 100 (2010) 179.
[64] T.G. Xu, L.W. Zhang, H.Y. Cheng, Y.F. Zhu, Chem. Rev. 101 (2010) 382.
[65] S. Sun, L. Gao, Y. Liu, Appl. Phys. Lett. 96 (2010) 083113.
[66] E. Gao, W. Wang, M. Shang, J. Xu, Phys. Chem. Chem. Phys. 13 (2011) 2887.
[67] R. Czerw, B. Foley, D. Tekleab, A. Rubio, P.M. Ajayan, D.L. Carroll, Phys. Rev. B 66 (2002) 033408.
[68] N. Yang, J. Zhai, D. Wang, Y.S. Chen, L. Jiang, ACS Nano 4 (2010) 887.
[69] D. Bahnemann, C. Kormann, M. Hoffmann, J. Phys. Chem. 91 (1987) 3789.
[70] C. Hu, Y.Z. Wang, H.X. Tang, Appl. Catal. B 30 (2001) 277.
[71] Y.B. Tang, C.S. Lee, J. Xu, Z.T. Liu, Z.H. Chen, Z.B. He, Y.L. Cao, G.D. Yuan, H.S. Song, L.M. Chen, L.B. Luo, H.M. Cheng, W.J. Zhang, I. Bello, S.T. Lee, ACS Nano 4 (2010) 3482.
[72] X.G. Chen, Y.Q. He, Q. Zhang, L.J. Li, D.H. Hu, T. Yin, J Mater. Sci. 45 (2010) 953.